



1 A Theory of Earthquake Prediction

2

3 Jeen-Hwa Wang

4 Institute of Earth Sciences, Academia Sinica, Taipei, Taiwan, ROC

5 E-mail: jhwang@earth.sinica.edu.tw

6

7

8

9 Abstract

10 In this study, the pre-seismic strain of an earthquake is considered as a fundamental
11 and important precursor. Based on the Voight's equation for material failure, we
12 theoretically investigate the physical basis on predicting the failure time, magnitude,
13 and location of a forthcoming earthquake in terms of pre-seismic strains generated on
14 or near the related fault where the event will happen. The $\log(T)-M$ relationship is
15 built up. Results exhibit that the failure time depends on the strain rate and two
16 parameters of the Voight's equation; while the magnitude is associated with the
17 precursor time, two parameters of the Voight's equation, and the exponent of the
18 scaling law between the strain and the fault length. The location of the forthcoming
19 earthquake may be qualitatively estimated from the localities of observation sites
20 where the pre-seismic strains are observed. In addition, the anomalous geoelectric and
21 geochemical signals prior to earthquakes are also taken into account as precursors.
22 Their $\log(T)-M$ relationships are derived. The precursor times of geoelectric signals
23 and those of the geochemical signals are, respectively, the same and shorter than that
24 of the pre-seismic strains.

25

26 **Keywords:** Earthquake prediction, strain, failure time, magnitude, location,
27 Voight's equation, fault length

28



29 **1 Introduction**

30

31 The ruptures of earthquakes, especially for large ones, are usually preceded by
32 complex physical and chemical processes which may produce the so-called precursors
33 (e.g., Atkinson, 1984; Main and Meredith, 1989; Main, 1999; Zaccagnino and
34 Doglioni, 2022). Hence, a significant way to reduce seismic hazards is the prediction
35 of forthcoming earthquakes based on observations of reliable precursors. Since Milne
36 (1880) first addressed this viewpoint in the nineteenth century, earthquake prediction
37 has been a challenging problem for earthquake scientists (e.g., Knopoff, 1996). Aki
38 (1989, 2009) assumed that earthquakes are predictable and earthquake scientists
39 should inform the probability of the occurrence of an earthquake with a specified
40 magnitude, place, and time window to the government and the public for mitigating
41 hazards. Although the earthquake prediction seems successful for few large events,
42 including the 1975 Haicheng, China, earthquake (cf. Wang et al., 2006), it has been
43 long a debatable problem of earthquake science. Numerous earthquake scientists
44 address that earthquakes can be predicted, but some others stand for the opposite
45 viewpoint (e.g. Geller, 1997; Geller et al., 1997). The latters were mainly based on the
46 reasons that the brittle crust is quite disordered and complicated (cf. Savage et al.,
47 2010) and it sometimes exists in the critical state (cf. Bak, 1996). The two conditions
48 will reduce the predictability of forthcoming earthquakes. However, disorder and
49 complexity within a single fault could be much lower than those in the brittle crust or
50 a fault system. A fault could be at the subcritical state (cf. Atkinson, 1984; Main and
51 Meredith, 1989) before its failure occurs. Hence, it is still significant to explore an
52 acceptable, workable model for predicting the failure time, t_f , the magnitude, M , and
53 the source area of a forthcoming earthquake from observed precursors, especially for
54 a single fault.

55 Although reliable precursors may provide us a clue to judge whether or not an
56 earthquake will happen in an area, the observations of precursors that are merely on
57 the reduction side of science (see Kuhn, 1962) thus cannot be directly applied to
58 predict anything. Hence, earthquake scientists need workable theories or models,
59 which are on the deduction side, for prediction. Up to date, the reduction side is much
60 stronger than the deduction one on the earthquake prediction research. This cannot
61 make earthquake prediction be successful. A major effort is still needed in the



62 scientific community in order to advance physical theories and models towards the
63 great goal of earthquake prediction. One of the most important matters is
64 the construction of physico-chemical models for respective precursors or even a
65 unified model for all precursors. Through the comparison between the observations
66 and the models, earthquake scientists could obtain the optimum ones for respective
67 precursors or the optimum unified one. Based on the optimum models or the optimum
68 unified one, earthquake scientists may be capable of predicting an earthquake,
69 including its location, time window, and magnitude as mentioned above. Of course,
70 such a model could be region-dependent, because different tectonic and geological
71 conditions will influence the parameters of the model.

72 Reid's elastic rebound theory (Reid, 1910) assumes that the loading stress and slip
73 on a fault are the major factors in causing an earthquake rupture. Numerous authors
74 (e.g., Dieterich, 1978; Lomnitz and Lomnitz-Adler 1981; Kostrov and Das, 1982;
75 Main, 1988, 1999; Scholz, 1990) assumed that the pre-seismic stress, σ , and slip, u (or
76 strain, ε), on a fault are two important factors in influencing the generation of
77 precursors. Anomalous pre-seismic displacements or strains near the faults have been
78 observed before numerous earthquakes. Tsubokawa et al. (1964) first measured
79 pre-seismic displacements at several inland sites before the June 16 1964 M7.5
80 Niigata, Japan, earthquake. Kanamori (1973, 1996) reported pre-seismic release
81 associated with forthcoming major earthquakes, especially in Japan. Yu et al. (2001)
82 reported the pre-seismic displacements on the near-fault stations before the September
83 20 1999 M7.6 Chi-Chi, Taiwan, earthquake. Papazachos et al. (2002) found
84 accelerating pre-seismic crustal deformation before large earthquakes in the Southern
85 Aegean area. Sarkar (2011) observed possible accelerated Benioff strains prior to
86 large earthquakes in the Sistan Suture Zone of Eastern Iran. These studies confirm the
87 significance and importance of pre-seismic slip or strain on either earthquake
88 prediction or assessment for forthcoming earthquakes. These studies confirm the
89 significance and importance of pre-seismic slip or strain on earthquake prediction or
90 assessment of forthcoming earthquakes.

91 Laboratory experiments reveal that σ and u are time-varying (Atkinson, 1984;
92 Rudnicki, 1988; Main and Meredith, 1989). While, the slip as well as the strain
93 increased very slowly with time from the initial time t_0 to a particular time t_c and then
94 increased rapidly from t_c up to the failure time t_f when an earthquake happens This is



95 the so-called quasi-static subcritical crack growth (SCG) model (Atkinson, 1984,
96 1987; Atkinson and Meredith, 1987) which is usually represented by the Charles law
97 (e.g., Das and Scholz, 1981; Main, 1988, 1999). Das and Scholz (1981) used this
98 model with Charles law to describe the acceleration of a crack tip from an initially
99 slow (sub-critical) rate due to stress corrosion to rapid remarkable rupture under
100 increasing stresses. They predicted the failure time which depends on initial
101 conditions on a fault, such as crack length, crack-tip velocity, residual frictional stress
102 following a previous earthquake, stress-corrosion index, and the rate of stress input.
103 Main (1988) applied a similar theory to predict the occurrence time of an event. His
104 model may quantitatively explain the decrease of failure time in the crust in terms of
105 decreases in the residual stress due to increasing heat flow, coupled with increases in
106 both stress-input rates and density of nucleation points for rupture initiation. The
107 model also predicts progressively increasing failure times for normal, strike-slip, and
108 thrust faults under similar conditions. Wang (2021a,b; 2023) and Wang et al. (2016)
109 classified the long-term, intermediate-term, short-term, and immediate-term
110 precursors based on the SCG (subcritical crack growth) model as mentioned above.

111 From rock mechanic experiments, Voight (1988, 1989) proposed a nonlinear
112 rate-dependent law for material failure:

113

$$114 \quad X_{tt} - aX_t^{-\alpha} = 0 \quad (1)$$

115

116 where X is an observable quantity, X_{tt} and X_t denote d^2X/dt^2 and dX/dt , respectively, a
117 is a constant, and α is the scaling exponent of the model. Based on rock mechanics, X
118 may be interpreted in terms of conventional geodetic observations (e.g., length change,
119 fault slip, strain or angular change), seismic quantities (e.g., the square root of
120 cumulative energy release or Benioff strain) or geochemical observations (such as gas
121 emission rates or chemical ratios). The parameter α varies with rock materials and
122 also depends on the temperature. Eq. (1) is called the Voight's equation hereafter.
123 Some authors (e.g., Varnes, 189; Kilburn and Voight, 1998) compared Eq. (1) with
124 the Charles law for the SCG model. Essentially, the Voight's equation is similar to the
125 Charles law. The Voight's equation has been applied to predict the failure time of an
126 earthquake based on the accelerated Benioff strain (e.g., Bufe and Vanus, 1993;
127 Bowman et al., 1996) and the accelerating strain (e.g., Main, 1999). In addition, Main



128 (1999) also studied the failure times of earthquakes by considering constitutive rules
129 of a simple percolation model (e.g., Stauffer and Aharony, 1994). However, they did
130 not predict the magnitude of a forthcoming earthquake.

131 The pre-seismic strains observed on or near a fault are directly related to the stress
132 and slip on the fault zone. Define $T=t_f-t_0$, where t_0 is the initial occurrence time of the
133 precursor, be the precursor time (see Wang et al., 2016; Wang, 2021a,b). In this study,
134 we will propose a theory to predict the failure time, t_f , magnitude, M , and location of a
135 forthcoming earthquake and to investigate the relationship between the precursor time
136 and earthquake magnitude from the pre-seismic and co-seismic strains based on the
137 Voight's equation. In addition, the theory can be also applied to other kinds of
138 precursors.

139

140 **2 Voight's Equation**

141

142 From the results obtained from the rock mechanics experiments, Voight (1988)
143 proposed the empirical equation, i.e., the so-called Voight's equation, to describe rate-
144 dependent material failure. The Voight's equation has been considered as a
145 fundamental physical law governing diverse forms of material failures (e.g. Voight,
146 1988, 1989). It is a more general form of Charles' law (Main, 1999). Like several
147 authors (e.g., Das and Scholtz, 1981; Main, 1988, 1999), I assume that this empirical
148 equation can be applied to real earthquakes. In addition, this empirical equation has
149 been applied to volcanic eruptions (Voight, 1988b; Cornelius and Voight, 1995;
150 Kilburn and Voight, 1998).

151 If X in Eq. (1) is taken to be the strain, ε , on a fault, the final stages of failure under
152 steady conditions of a rock in compression would show a proportionality between the
153 logarithm of creep acceleration and the logarithm of creep velocity. Integrating Eq. (1)
154 gives the expression for the strain rate, ε_t , and strain acceleration, ε_{tt} , on a fault zone.
155 In the followings, the strain and strain rate at the initial time, t_0 , are denoted by ε_0 and
156 ε_{t0} , respectively; while those at the failure time, t_f , are shown by ε_f and ε_{tf} ,
157 respectively. The solution is dependent on the scaling exponent α . For $\alpha=1$, the strain
158 rate is

159

$$160 \quad \varepsilon_t = \varepsilon_{t0} e^{\alpha(t-t_0)}. \quad (2)$$



161

162 For $\alpha < 1$, the strain rate is

163

164
$$\varepsilon_t = [a(1-\alpha)(t-t_0) + \varepsilon_{t0}^{(1-\alpha)}]^{1/(1-\alpha)}. \quad (3)$$

165

166 For $\alpha > 1$, the strain rate is

167

168
$$\varepsilon_t = [a(\alpha-1)(t_f-t) + \varepsilon_{tf}^{(1-\alpha)}]^{1/(1-\alpha)}. \quad (4)$$

169

170 These equations remarkably reveal that ε_t increases with time and thus there is not an
171 upper bound of ε_t . The value of ε_t can be evaluated from the first two equations for
172 $\alpha \leq 1$ and cannot be resolved from the third equation for $\alpha > 1$. It seems that there is a
173 singular point at t_f for $\alpha > 1$. At the singular point, a rock fracture or an earthquake
174 would happen. An example of numerical results can be seen in Voight's (1989) Figure
175 2. Since ε is integrated from ε_t , there is not an upper bound value for ε when $\alpha \leq 1$.

176 We may further solve the time-dependent strain $\varepsilon(t)$ through double integration of
177 Eq. (1). For $\alpha > 1$ and $\alpha \neq 2$, the result is

178

179
$$\varepsilon(t) - \varepsilon_0 = \{[a(\alpha-1)(t_f-t_0) + \varepsilon_{tf}^{(1-\alpha)}]^\eta - [a(\alpha-1)(t_f-t) + \varepsilon_{tf}^{(1-\alpha)}]^\eta\} / a(\alpha-2) \quad (5)$$

180

181 where η represents $(2-\alpha)/(1-\alpha)$. For $\alpha > 1$ and $\alpha \neq 2$, the values of η are: (1) $\eta < 0$ as
182 $1 < \alpha < 2$; and (2) $\eta > 0$ as $\alpha > 2$. From the theoretical studies made by Main (1998), we
183 can see that the condition of the existence of accelerating strain for generating an
184 earthquake is $1 < \alpha < 2$, thus leading to $\eta < 0$. This condition will be used hereafter.

185

186 3. Theory of earthquake prediction

187

188 According to the Voight's equation, I assume that it is possible to predict the failure
189 time of a forthcoming earthquake from the observed pre-seismic strains measured on
190 or near the fault along which the event will occur. The prediction of the failure time is
191 based on Eq. (4) and the prediction of the magnitude is based on Eq. (5). The location
192 of the event should be near the sites of observing the pre-seismic strains. The theory



193 of earthquake prediction proposed in this study is described below.

194

195 **3.1 Predicting the Failure Time of a Forthcoming Earthquake**

196

197 Since the condition $1 < \alpha < 2$ is considered here, we will only take Eq. (4) in the
198 followings. Due to $1 - \alpha < 0$, the strain rate, ε_{tf} , at the failure time should be much larger
199 than 1 strain/sec and thus $\varepsilon_{tf}^{1-\alpha}$ is much smaller than 1 strain/sec. This makes Eq. (4)
200 become

201

202
$$\varepsilon_t = [a(\alpha-1)(t_f-t)]^{1/(1-\alpha)}. \quad (6)$$

203

204 The time variations in ε_t from Eq. (6) for $\alpha=1.5$, 1.6, and 1.7 when $a=0.5$ are
205 displayed in Fig. 1 in which ε_t is normalized by the maximum value of ε_t for the three
206 cases. In the figure, the three curves intersect to one another at a point with $t=t_c$.
207 When $t < t_c$, ε_t increases slowly with time and increases with α ; while when $t > t_c$, ε_t
208 increases rapidly with time and decreases with increasing α .

209 From Eq. (6), we propose a method to explore the possibility of predicting the
210 failure time, t_f of a forthcoming earthquake. Since the values of three model
211 parameters t_f , a , and α , must be solved, those of ε_t at three time instants should be
212 given. Considering the pre-seismic strain rates, i.e., ε_{t1} , ε_{t2} , and ε_{t3} , at three time
213 instants, i.e., t_1 , t_2 , and t_3 , respectively. An example for $\alpha=1.6$ with $a=0.5$ is shown in
214 Fig. 2 in which ε_t is normalized by the maximum value of ε_t . Inserting ε_{tj} and t_j ($j=1$,
215 2, and 3) into Eq. (6) yields

216

217
$$\varepsilon_{tj} = [a(\alpha-1)(t_f-t_j)]^{1/(1-\alpha)} \quad (j=1, 2, 3). \quad (7)$$

218

219 This leads to

220

221
$$t_f = t_j + \varepsilon_{tj}^{1-\alpha} / a(\alpha-1) \quad (j=1, 2, 3). \quad (8)$$

222

223 From Eq. (8) for ε_{t1} at t_1 and ε_{t2} at t_2 , we have

224



225 $t_2-t_1=[\varepsilon_{t2}^{(1-\alpha)}-\varepsilon_{t1}^{(1-\alpha)}]/a(\alpha-1)$ (9a)

226

227 or

228

229 $a(\alpha-1)=[\varepsilon_{t2}^{(1-\alpha)}-\varepsilon_{t1}^{(1-\alpha)}]/(t_2-t_1).$ (9b)

230

231 Similarly, from Eq. (8) for ε_{t1} at t_1 and ε_{t3} at t_3 we have

232

233 $t_3-t_1=[\varepsilon_{t3}^{1/(1-\alpha)}-\varepsilon_{t1}^{1/(1-\alpha)}]/a(\alpha-1)$ (10a)

234

235 or

236

237 $a(\alpha-1)=[\varepsilon_{t3}^{(1-\alpha)}-\varepsilon_{t1}^{(1-\alpha)}]/(t_3-t_1).$ (10b)

238

239 Define two functions in term of α , i.e., $F_{21}(\alpha)=[\varepsilon_{t2}^{(1-\alpha)}-\varepsilon_{t1}^{(1-\alpha)}]/(t_2-t_1)$ and $F_{31}(\alpha)=$
240 $[\varepsilon_{t3}^{(1-\alpha)}-\varepsilon_{t1}^{(1-\alpha)}]/(t_3-t_1)$. From Eqs. (9b) and (10b), $F_{21}(\alpha)$ and $F_{31}(\alpha)$ are the same
241 because they are both equal to $a(1-\alpha)$. We may evaluate the value of α directly from
242 the equality $F_{21}(\alpha)=F_{31}(\alpha)$. We first plot the difference of the two functions for
243 $1<\alpha<2$. An example of $F_{21}(\alpha)-F_{31}(\alpha)$ in terms of $\alpha=1.6$ is shown in Fig. 3 in which
244 the normalized values of $F_{21}(\alpha)-F_{31}(\alpha)$, i.e., $(F_{21}(\alpha)-F_{31}(\alpha))/(F_{21}(\alpha)-F_{31}(\alpha))_{\max}$, is
245 given. The condition for the existence of the value of α to make $F_{21}(\alpha)=F_{31}(\alpha)$ is that
246 the curve of $F_{21}(\alpha)-F_{31}(\alpha)$ must intersect the horizontal line with $F_{21}(\alpha)-F_{31}(\alpha)=0$ at
247 a point with a certain value of α as displayed in Fig. 3. After the value of α has been
248 evaluated, we may calculate the value of a from either $a=F_{21}(\alpha)/(1-\alpha)$ or $a=F_{31}(\alpha)/$
249 $(1-\alpha)$. Then, we may evaluate the failure time of the forthcoming earthquake from Eq.
250 (7) by using the following expression:

251

252 $t_f=t_j+\varepsilon_{tj}^{1/(1-\alpha)}/a(\alpha-1) \quad (j=1, 2, 3).$ (11)

253

254 The difference between the occurrence time of a precursor and the failure time of the
255 forthcoming earthquake is called the precursor time (e.g., Wang et al., 2016; Wang,
256 2021a,b) and is denoted by T hereafter. For the present case, the occurrence time of



257 the precursor and the failure time of the forthcoming earthquake are t_o and t_f ,
258 respectively, thus leading to $T=t_f-t_o$.

259

260 **3.2 Prediction of the Magnitude of a Forthcoming Earthquake**

261

262 Based on the evaluated precursor time, T , it is possible to predict the magnitude of an
263 earthquake by using Eq. (5). It first needs to discuss the value of initial strain ε_o . After
264 the ruptures of last earthquake on a fault, the fault usually continues to slide with the
265 relative movement speed of regional plates until the occurrence of the next event. If
266 the moving speed is v_p , the strain rate, ε_t , is v_p/L where L is the fault length on a fault.
267 Here the value of $\varepsilon_t \delta t$ with the time unit δt of 1 second is taken to be ε_o . The value of
268 ε_t is commonly 10^{-6} strain/year around the world (e.g., Scholz et al., 1973; Turcotte
269 and Schubert, 1982; Yu et al., 2001). For an example, the value of ε_t is
270 $0.25 \times 10^{-6}/\text{yr} = 1.90 \times 10^{-13}/\text{sec}$ for the San Andres fault (cf. Turcotte and Schubert,
271 1982), thus leading to $\varepsilon_o = 1.90 \times 10^{-13}$ which is much smaller than 1. This makes us
272 able to take $\varepsilon_o = 0$ in this study. Figures 1 and 2 reveal $\varepsilon_t \gg 1$. According to the two
273 conditions, Eq. (5) becomes

274

$$275 \varepsilon(t) = \{[a(\alpha-1)T]^\eta - [a(\alpha-1)(t_f-t)]^\eta\}/a(\alpha-2). \quad (12)$$

276

277 Voight (1988, 1989) took $a=0.5$ for studying the results of his rock mechanic
278 experiments. Hence, the values of ε_t is about a few strain/day or 10^{-4} strain/sec for
279 laboratory earthquakes. As mentioned above, the values of pre-seismic strain, ε , much
280 before the occurrences of natural earthquakes are very small. Hence, the value of
281 parameter a should be small for natural earthquakes. Nevertheless, the value of a is
282 still taken to be 0.5 in Fig. 4 which illustrates the time variations in ε from Eq. (12)
283 for $\alpha=1.5, 1.6$, and 1.7 . In the figure, ε is normalized by the maximum value of the
284 three cases. Like Fig. 1, Fig. 4 shows that the three curves intersect to one another at a
285 point with $t=t_c$. When $t < t_c$, ε_t increases slowly with time and increases with α ; while
286 when $t > t_c$, ε_t increases rapidly with time and decreases with increasing α .

287 The earthquake ruptures at $t=t_f$ when the strain is ε_f , which is

288



289 $\varepsilon_f = [a(\alpha-1)T]^\eta/a(\alpha-2)$ (13)

290

291 from Eq. (12). This is the upper bound of $\varepsilon(t)$ for $\alpha>1$ and $\alpha\neq 2$. This upper bound is
292 dependent on both the parameters of fault-zone materials and precursor time.
293 Re-organizing Eq. (13) and taking the logarithm on the two sides of the re-organized
294 equation yield

295

296 $\log(T) = \log\{[a(\alpha-2)\varepsilon_f]^{1/\eta}/[a(\alpha-1)]^\eta\}$. (14)

297

298 Eq. (14) gives

299

300 $\log(T) = \log\{[a(\alpha-2)]^{1/\eta}/a(\alpha-1)\} + \log(\varepsilon_f)/\eta$. (15)

301

302 This represents the power-law scaling relationship between T and ε_f , i.e., $T \sim \varepsilon_f^{1/\eta}$.

303 Since the rupture duration of an earthquake is short, we may consider ε_f as the
304 average strain over the ruptured area after failure. Shaw (2023) inferred the scaling
305 law for ε_f versus the fault length of an earthquake, L , in the following form: $\varepsilon_f = \lambda L^{-1/2}$.

306 This leads to

307

308 $\log(\varepsilon_f) = \log(\lambda) - \log(L)/2$, (16)

309

310 where λ is a region-dependent constant. Several authors (e.g., Kanamori and
311 Anderson, 1976; Wells and Coppersmith, 1994; Leonard, 2010; Thingbaijam et al.,
312 2017; Wang, 2018; Shaw, 2023) inferred the scaling law for L versus M , which is the
313 earthquake magnitude (usually the seismic-wave magnitude, M_s , or the moment
314 magnitude, M_w), in the following form:

315

316 $\log(L) = \chi + M/2$ (17)

317

318 where χ is a constant depending on tectonic and geological conditions. Combination
319 of Eqs. (15), (16), and (17) leads to the $\log(T)-M$ relationship:

320

321 $\log(T) = C + A M$ (18)



322

323 where two new parameters are $C = \log\{[a(\alpha-2)]^{1/\eta}/a(\alpha-1)\} + [\log(\lambda) - \chi/2]/\eta$ and $A = -1/4\eta$.

324 Obviously, A is positive due to $\eta < 0$ because of $1 < \alpha < 2$ as mentioned above. This
325 results in a positive correlation between T and M . When T is known, the value of M
326 for the forthcoming earthquake may be evaluated from Eq. (18), i.e., $M = [\log(T) - C]/A$.
327 From past studies (cf. Wang, 2021b, 2023; and cited references therein), the values of
328 A from observations are all smaller than 1. This leads to $\alpha < 1.8$ and thus the values of
329 α for natural earthquakes could be in the range 1.0 to 1.8.

330

331 **3.3 Predicting the Location of a Forthcoming Earthquake**

332

333 As mentioned by Aki (1989), the earthquake scientists should provide the location of
334 the forthcoming earthquake to the public. Hence, predicting the potential location of
335 the forthcoming earthquake is also important for seismic hazard mitigation. When the
336 stations on which the pre-seismic strains are observed are close to a known active
337 fault, it is very possible to assess the occurrence of the forthcoming earthquake along
338 the fault. On the other hand, when the station site is not close to a known active fault
339 or within a complicated active fault system, it needs other precursors, for example,
340 b -value anomalies (e.g., Wang et al., 2016), foreshock activities (e.g., Chen and Wang,
341 1984; Chen et al., 1990; Gulia and Wiemer 2019; Zaccagnino et al., 2024),
342 geochemical anomalies (e.g., Walia et al., 2009; Fu and Lee, 2018) electromagnetic
343 anomalies (e.g., Ohta et al., 2005, Hayakawa et al., 2006; Hayakawa and Hobara,
344 2010; De Santis et al., 2019) etc., for helping earthquake scientists to make correct
345 assessment. Hence, researchers have also suggested other methods to judge the
346 possible location of the forthcoming earthquake. Seismologists (e.g., Rundle et al.,
347 2000; Wu et al., 2012) suggested a method to assess the location from seismicity
348 pattern. For some strike-slip and normal earthquakes, seismologists can assess the
349 possible location of the mainshock from its foreshocks (e.g., Chen et al., 1990).
350 Geochemists (e.g., Walia et al., 2009; Fu and Lee, 2018) suggest a method just like
351 that used by seismologists to locate an earthquake from the differences between travel
352 times of P - and those of S -waves recorded at three stations. They took the occurrence
353 times of geochemical precursors, recorded at three different stations to evaluate the
354 optimal location of a forthcoming earthquake. Geophysicists (e.g., Ohta et al., 2005,



355 Hayakawa et al., 2006; Hayakawa and Hobara, 2010) suggest the goniometric method
356 to assess the location of the forthcoming event by detecting the directions of ULF
357 emissions from the observational stations to the earthquake epicenter. These methods
358 seem acceptable.

359

360 **4 Discussion**

361

362 **4.1 On the Theory for the Pre-seismic Strains**

363

364 Fig. 1 shows that the strain rate, ε_t , monotonically increases with time. From Fig. 1,
365 Eq. (1) will lead to an increase in the strain acceleration, ε_{tt} , with time. For the time
366 variation as displayed in Fig. 1, at a certain time instant, larger α yields higher ε_t .
367 Meanwhile, there are two steps more or less separated at a particular time instant, t_c ,
368 which is shorter than t_f and not displayed in the figure. The two steps are: ε_t first
369 slowly with time when $t < t_c$ and then rapidly with time when $t > t_c$. Such a particular
370 time appears earlier for large α than for small α . The second step is the existence of
371 accelerating strain before a forthcoming earthquake from the theoretical studies by
372 Main (1998). From observations of foreshocks, some authors (e.g., De Santis et al.,
373 2015; and Cianchini et al., 2020) applied the revised accelerated moment release
374 model to foreshocks revealing an acceleration pointing to the mainshock. Their model
375 is similar to the present one. Since there is background noise in practical observations,
376 the anomalous strain rate can be measured only in the second step. Like Fig. 1, Fig. 4
377 also illustrates the similar time variation in the strain, ε . For all cases in Fig. 4, there
378 are also two steps separated at a particular time instant, t_c : ε first slowly with time
379 when $t < t_c$ and then rapidly with time when $t > t_c$. Unlike Fig. 1, such a particular time
380 is almost the same for all α 's in use. Meanwhile, in Fig. 4 ε increases with α when t is
381 smaller than such a particular time; while ε decreases with increasing α , when t is
382 larger than such a particular time. This is the main difference between Fig. 1 and Fig.
383 4. In addition, larger α produces lower ε_t as t is approaching t_f in Fig. 4. This means
384 that the strain during a forthcoming earthquake increases with decreasing α .

385 The theory of predicting the failure time of a forthcoming earthquake proposed by
386 this study is basically similar to that used by Das and Scholz (1981) based the Charles



387 law and that suggested by Main (1988) based on the Voight equation. One difference
388 between this method and theirs is that the values of strain rate at three time instants
389 are taken in this study, while only those of pre-slip at two time instants were
390 considered in theirs. This is due to a reason that they assumed that the model
391 parameters of either Charles law or Voight's equation have been already known,
392 while those in this study are originally unknown and must be estimated from the
393 observations.

394 Equation (18) exhibits the $\log(T)-M$ relationship based on pre-seismic strains.
395 Tsubokawa (1969, 1973) first obtained a linear relation between the precursor time of
396 crustal movement and mainshock magnitude for Japanese earthquakes in the form:
397 $\log(T) = -1.88 + 0.79M$, with $C = -1.88$ and $A = 0.79$. His observations somewhat confirm
398 the existence of the $\log(T)-M$ relationship. This makes us capable of predicting the
399 magnitude of a forthcoming earthquake when the precursor time has been evaluated
400 from observations. Although the earthquakes used by Tsubokawa (1969, 1973)
401 occurred on different fault zones, his $\log(T)-M$ relationship with the values of C and
402 A represents the average characteristics of crustal deformations in Japan. In general,
403 the parameters a and α of Voight's equation and λ and χ of the scaling laws of faults
404 vary from area to area. Hence, the $\log(T)-M$ relationships might be distinct in
405 different fault systems.

406 Wang (2023) correlated the precursor time to the earthquake energy. The
407 Gutenberg-Richter's energy-magnitude law of earthquakes (Gutenberg and Richter,
408 1942, 1956) is: $\log(E_s) = 11.8 + 1.5M$ in which E_s is the seismic-wave energy (in ergs)
409 and M is commonly the surface-wave magnitude, M_s . From the law, he obtained the
410 correlation: $M \sim (2/3)\log(E_s)$. In addition, from $\log(T) = C + AM$ he got $\log(T) \sim AM \sim$
411 $(2A/3)\log(E_s)$. Since $E_s = \xi \Delta E$ where ΔE is the strain energy of an earthquake and ξ
412 (< 1) is the seismic efficiency, Wang (2004) obtained $T \sim \Delta E^{A\xi/3}$. This indicates that the
413 precursor time is dependent on the strain energy of the forthcoming earthquake. The
414 seismic efficiency that depends on the physical and chemical properties of the
415 fault-zone rocks (Knopoff, 1958; Kanamori and Heaton, 2000; Wang, 2009) may also
416 influence T . A high seismic efficient will yield a long precursor time.

417

418 **4.2 Application of the Theory to Other Earthquake Precursors**

419



420 **4.2.1 The $\log(T)$ - M relationships for other Precursors**

421

422 In order to measure the pre-seismic strains, the strain-meters should be installed on or
423 much near the fault. When a strain-meter has not installed on or near the fault on
424 which a forthcoming earthquake will happen, it is hence necessary to use other kinds
425 of precursors which are directly or indirectly caused by the pre-seismic fault slip or
426 strains for predicting the earthquake. In other word, it is much significant to explore
427 the application of the present theory on the prediction of t_f and M of a forthcoming
428 earthquake based on other kinds of precursors in practice. The present theory can be
429 applied to other kinds of precursors, and thus the $\log(T)$ - M relationships exist for
430 these precursors. It is significant to apply the above-mentioned theory to predict the
431 failure time and magnitude of a forthcoming earthquake based on other kinds of
432 precursors.

433 The $\log(T)$ - M relationships have been recognized from the observations of
434 different kinds of precursors for a long time (Rikitake 1975a; Wang, 2021a,b, 2023;
435 and cited references therein). From the plot of T (in days) versus M for five precursors,
436 i.e., crustal movements, electric resistivity, radon (denoted as Rn hereafter) emission,
437 v_p/v_s anomaly, and b -value of Gutenberg-Richter frequency-magnitude law
438 (Gutenberg and Richter, 1944). From 30 world-wide earthquakes, Scholz *et al.* (1973)
439 inferred a relationship: $M_s = -5.81 + 1.55 \log(T)$ (T in days) or $\log(T) = 3.75 + 0.65 M_s$. For
440 the precursors of crustal deformations and seismic-wave velocities, Whitcomb *et al.*
441 (1973) obtained $\log(T) = -1.92 + 0.80 M_s$ (T in days). Rikitake (1975b) obtained $\log(T) =$
442 $-1.83 + 0.76 M_s$ (T in days). He also stressed that the $\log(T)$ - M_s relationships are
443 different for different groups of precursors. Rikitake (1979, 1984) divided a large data
444 set of 391 cases of precursors into three classes. He obtained $\log(T) = -1.01 + 0.60 M_s$ for
445 the first class including 192 cases and $\log(T) = -1.0$ for the second class. He did not
446 report any relationship for the third class for foreshocks, tilt and strain, and earth's
447 currents. Smith (1981, 1986) obtained the following
448 relationship: $\log(T) = 1.42 + 0.30 M_s$ (T in years) from the data of abnormal b -values for
449 earthquakes in New Zealand. Ding *et al.* (1985) obtained $\log(T) = -0.34 + 0.38 M_s$ (T in
450 years) for various precursors proceeding large Chinese earthquakes. From the b -value
451 anomalies for 45 world-wide earthquakes with $3 \leq M_s \leq 9$, Wang *et al.* (2016) obtained
452 $\log(T) = (2.02 \pm 0.49) + (0.15 \pm 0.07) M_s$ (T in years).

453 From the previous description, it is clear that the $\log(T)$ - M relationships are



454 different for distinct kinds of precursors and also region-dependent. These results
455 strongly suggest regional-dependence of C and A of Eq. (18). Clearly, C is influenced
456 by several parameters, while A is controlled only by the scaling exponent, α , of the
457 fault-zone materials. Hence, A is an important indicator of the relationship. The
458 previous studies lead to two interesting points. First, for the same forthcoming
459 earthquake, different kinds of precursors may have different precursor times due to
460 distinct values of C , but the same value of A . Secondly, for the forthcoming
461 earthquakes that have the same magnitude and occur at different fault zones, different
462 kinds of precursors may have different precursor times due to distinct values of both
463 C and A .

464 We will explore the theoretical basis for two kinds of precursors in the followings.
465 The first kind of precursors is the geoelectric signals which are yielded almost within
466 the fault zone where the forthcoming earthquake will happen, and the other is the
467 geochemical signals which might occur on the sites that are somewhat far away from
468 the fault zone. The mechanisms to generate the two kinds of signals will be described
469 below.

470

471 **4.2.2 For the Geoelectric Precursors**

472

473 Changes or anomalies of geoelectric signals have been observed prior to earthquakes
474 for a long time (cf. Hayakawa and Hobara, 2010; and cited references therein).
475 Geoelectric signals are associated with pre-seismic slip on a fault where a
476 forthcoming earthquake will happen. It is necessary to build up a comprehensive
477 model that presents the lithosphere-ocean-atmosphere-ionosphere-magnetosphere
478 coupling to interpret the generation of geoelectric precursors (Potirakis et al., 2017;
479 Ouzounov et al., 2018; and cited references therein). Several proposed models are: (1)
480 a model to present Rn ionization and charged aerosol and change of load resistance in
481 the global electric circuit (Ouzounov et al., 2018; Pulinets and Ouzounov, 2018; and
482 cited references therein); (2) a model to show coupling between stressed rocks and the
483 atmosphere-ionosphere system (e.g., Kuo et al., 2011, 2014) based on experimental
484 results of stress-induced charges made by Freund (2002); (3) a model to display
485 ionosphere dynamics with imposed zonal (west-east) electric field (Zolotov et al.,
486 2011, 2012; Namgaladze et al., 2012); and (4) a model of leakage of electric currents



487 from ocean into the crust having low electric resistivity (Madden and Mackie, 1996).
488 The existence of electric charges/currents on the Earth's ground or in the uppermost
489 crust is a necessary condition for these models. Several mechanisms, including
490 microfracturing (e.g., Ogawa et al., 1985; Molchanov and Hayakawa, 1995),
491 electrokinetic effect (e.g., Mizutani et al., 1976), streaming potentials (e.g., Bernard,
492 1992), piezoelectricity (e.g., Bishop, 1981; Sornette, 2001; Wang, 2021c),
493 triboelectricity/triboluminescence (e.g., Yoshida et al., 1998), confined pressure
494 changes (e.g., Fujinawa et al., 2002), the peroxy defect theory (Freund, 2002),
495 piezomagnetism (e.g., Sasai, 1979, 1980; Martin, 1980), etc. have been proposed to
496 explain electric charge generation within the fault zones.

497 Here, we show three examples to show the geoelectric and geomagnetic precursors
498 caused by pre- seismic ground electric currents. First, Whitworth (1975) proposed a
499 model of the motion of charged edge location (MCD). According to the MCD model,
500 numerous authors (e.g., Tzanis and Vallianatos, 2002; Venegas-Aravena et al., 2019)
501 assumed that an electric current density, J , generated within rocks under
502 compressional stress changes with time, i.e., $\sigma_t = d\sigma/dt$, can be represented by
503 $J = 2^{1/2}(q/\psi B_v)(\sigma_t/Y)$ where q is the linear charge density of edge dislocation, B_v is the
504 Burgers vector module, ψ (=1–3), which represents the dislocation number created by
505 compression and uniaxial tension within a rock (Whitworth, 1975; Vaillianatos and
506 Tzanis, 1998), and Y is the Young's effective module (Turcotte et al., 2003). Since the
507 quantity σ_t/Y may be replaced by the strain rate ε_t , the electric current density
508 becomes $J = 2^{1/2}(q/\psi B_v)\varepsilon_t$. The geoelectric field is $E = J/\theta_c$, where θ_c is the electric
509 conductivity, from the Maxwell equation. Meanwhile, the geomagnetic field at a
510 distance, r , from the electric current density is $|B| = \mu_B J / 2\pi r$, where μ_B is the
511 permeability of free space, from the Biot-Savart law (cf. Corson and Lorrain, 1962).
512 Clearly, E and B are both related to ε_t . Secondly, Enomoto (2012) obtained
513 $\log(J) = 0.5M + \log(5.1 \times 10^2 e k n h^2 D_c / \nu)$ (e =the electronic charge; k =a constant of
514 proportionality; n =the density of negatively charged gas molecules; h =the crack gap;
515 D_c =critical depth; and ν =the gas viscosity). This shows the correlation between J and
516 ε . Thirdly, some authors (e.g., Sornette, 2001; Wang, 2021c) studied the dependence
517 of ground electric field, E , on pre-seismic slip, u , in a fault zone in a one-dimensional
518 model with the spatial coordinate x based on the piezoelectricity and the Maxwell's
519 equations. The result is: $E = -i(c/\nu)^2(\kappa/\zeta)u$ where $i = (-1)^{1/2}$ is the imaginary number,



520 $v=(\mu/\rho)^{1/2}$ is the elastic wave velocity, ρ is the density (kg/m^3) of fault-zone rocks, and
521 c is the light speed ($=2.999\times10^8$ m/sec in free space), ζ is the piezoelectric coupling
522 coefficient between elastic field and electric field ($\zeta\approx2\times10^{-12}$ coulomb/ newton for
523 quartz), and κ is the wavenumber. Let L_o be the original length of a fault, thus leading
524 to $E=-i(c/v)^2(\kappa/\zeta)(u/L_o)L_o=-i(c/v)^2(\kappa L_o/\zeta)\varepsilon$. The three examples of geoelectric and
525 geomagn anomalies, thus leading to precursors of earthquakes. The precursor times of
526 GEM precursors should be the same as that of the pre-seismic strains. However,
527 Wang (2021a,b) reported different precursor times of electric field and magnetic field
528 even though they appeared before the same earthquake. It is necessary to explore the
529 reasons to cause such a difference in future.

530 The MCD model is put into the present theory to predict the failure time and
531 magnitude of a forthcoming earthquake. Inserting E_{ij} and t_j ($j=1, 2$, and 3) into Eq. (6)
532 yields

533

$$534 E_{ij}=F[a(\alpha-1)][(t_f-t_j)]^{(1-\alpha)} \quad (j=1, 2, 3). \quad (19)$$

535

536 This leads to

537

$$538 t_f=t_j+(E_{ij}/F)^{(1-\alpha)}/a(\alpha-1) \quad (j=1, 2, 3). \quad (20)$$

539

540 From Eq. (20), we may predict the failure time, t_f , of the forthcoming earthquake.
541 Since E increases with ε_i , their precursor times are the same and thus the precursor
542 time, T , is t_f-t_o . Theoretically, the precursor time of the pre-seismic geoelectric
543 precursor is the same as that of the pre-seismic fault strains. From T , we may predict
544 the magnitude of the forthcoming earthquake from Eq. (18), i.e., $M=[\log(T)-C]/A$.

545 In principle, the theory works well to predict the failure time of a forthcoming
546 earthquake by using the pre-seismic geoelectric signals. But, in practice there might
547 be a problem that the values of E_i cannot be observed accurately because of the
548 presence of unexpected noise due to thunderstorm, atmospheric abnormal phenomena,
549 and artificial effects. This problem should be very serious when $t < t_c$ because their
550 values are very small and cannot be observed. Hence, the observed data of geoelectric
551 signals must be carefully selected and corrected to remove noise. The visible
552 geoelectric signals should appear when $t > t_c$ because the signals are strong enough. In



553 addition, in principle E_i must be measured near the fault. But, the monitoring station
554 of geoelectric signals is usually not located near a fault where a forthcoming
555 earthquake will happen. The value of E_i measured at a station not close to the
556 epicenter should be slightly different from and weaker than near-fault one due to
557 attenuation. Nevertheless, the attenuation of geoelectric signals measured at several
558 time instants should be the same on the same station unless there are thunderstorm
559 and abnormal atmospheric phenomena between two time instants of different stations.

560

561 **4.2.3 For the Geochemical Precursors**

562

563 Numerous geochemical precursors are not observed at the localities near the
564 earthquake epicenters (Wang 2021a,b; and cited references therein) because the
565 observation stations are not installed at the sites near the epicenters. For example, Rn
566 concentration anomalies prior to an earthquake are often observed somewhat far away
567 from the epicenters because the measurement instruments are installed at hot-water
568 springs or water-wells which may be far away from the epicenters. Nevertheless, their
569 appearances are still related to the pre-seismic slip in the fault zones of forthcoming
570 events. We assume that the presence of Rn concentration anomalies in the
571 underground water might be associated with the spatial distribution of focal
572 mechanism of an earthquake. The spatial pattern of the fault mechanism of an
573 earthquake has four quarters: two for tension or dilatation and others for compression.

574 Kuo et al. (2010, 2019) reported a positive correlation between the temporal
575 variation in Rn concentrations and that of dilatational strains measured at the Antong
576 station for three events in southeastern Taiwan. The dilatational strains were related to
577 tensional quarters of focal mechanisms of the events as mentioned above. They
578 considered a model to explain Rn volatilization in an undrained fractured aquifer. This
579 model is simply described below. A small fractured aquifer situated in a brittle rock,
580 which is surrounded by a ductile formation in undrained conditions. When aquifer
581 recharge is weak and negligible, undrained conditions are valid. There is only a single
582 water phase in the aquifer before any precursory geochemical phenomenon appears.
583 When the regional stress increases, dilation of brittle rock could occur at a faster rate
584 than the rate of groundwater recharging into the newly created micro-cracks. As a
585 result, gas saturation and two phases (gas and water) develop in the aquifer. The radon
586 in groundwater volatilizes into the gas phase and the Rn concentration in groundwater



587 decreases. The model is mathematically represented by the following equation:

588

589
$$C_w/C_o = (HS_g + 1)^{-1} \quad (21)$$

590

591 where C_o is the initial Rn concentration (in pCi/L) in formation brine (salt water); C_w
592 is the equilibrium Rn concentration (in pCi/L) remaining in ground-water; S_g is the
593 gas saturation (in %); H is Henry's coefficient (dimensionless) for Rn. From the
594 rock-dilatancy model (Brace et al., 1966): $\varepsilon_v = S_g/(1/\phi)$ or $S_g = \varepsilon_v/\phi$ where ε_v and ϕ
595 denote, respectively, the (dimensionless) volumetric strain of the rocks beneath the
596 observation site and the initial fracture porosity before rock dilatancy. The volumetric
597 strain may be represented as $\varepsilon_1 + \varepsilon_2 + \varepsilon_3$ where ε_j is the strain along the j -th axis ($j=1, 2,$
598 and 3) (Turcotte and Schubert, 1982). This yields $S_g = (\varepsilon_1 + \varepsilon_2 + \varepsilon_3)/\phi$. Equation (19)
599 shows that C_w increases with decreasing S_g . Inside the brittle rocks underneath the
600 observation site, S_g increases with ε_v , thus leading to a decrease in C_w . The value of
601 ε_v inside the brittle rocks underneath the observation site will be induced by the strain
602 in the fault zone where the forthcoming earthquake will occur. Hence, the Rn
603 concentration changes are controlled by pre-seismic strains that occur in the related
604 fault zone.

605 Note that although we have considered a model to describe the production of
606 preseismic geochemical signals, the production processes could be more complicated
607 than the present model. Schirripa Spagnolo et al. (2024) addressed that preseismic
608 geochemical signal are produced by the transport of chemical markers throughout the
609 aquifers producing complex spatial circulations and alterations which can be
610 extremely difficult to grasp using just one single model. They also claimed that such
611 complex interactions among fault zones, host rocks upper and lower crustal volumes
612 produce a wide range feedback mechanisms. These problems are beyond the scope of
613 this study and need further investigations.

614 Of course, the time-dependent pre-seismic slip or strain on a fault along which a
615 forthcoming earthquake will happen can produce stress changes surrounding the fault
616 (Aki and Richards, 1980). This might induce some geochemical precursors which
617 occur on some places somewhat far away from the fault. Hence, such kinds of
618 precursors will appear more or less later than the pre-seismic slip or strain that
619 happened on the fault. This results in a shorter precursor time than that for the



620 pre-seismic slip or strain. Here, we consider a mechanical model to explain the
621 problem. Dobrovolsky et al. (1979) used a half space, during the preparation
622 processes of an earthquake, a zone of cracked rocks is formed in the focal area under
623 the tectonic loading, τ . The media inside the zone may be considered as a solid
624 inclusion with different moduli that are lower than that of the half space. The solid
625 inclusion re-distributes the stresses accompanied by deformations, including those on
626 the Earth's ground surface. Let V be the solid soft inclusion volume that is an ellipse
627 with a long-axis length of l_l and a short-axis length of l_s : $l_l > 1$ for $M \geq 5$ and $l_l = l_s$ for
628 $M < 5$, thus leading to $V = \pi l_l l_s^2 / 6$ for $M \geq 5$ and $V = \pi l_s^3 / 6$ for $M < 5$. The shear modulus of
629 the half space and that of the inclusion are μ and $\mu - \delta\mu$, respectively. The ratio $\delta\mu/\mu$ is
630 denoted by φ . Assuming that the zone of effective manifestation of the precursory
631 deformations is a sphere with the center at the epicenter of the forthcoming
632 earthquake under the shear stresses loaded at infinity. In the spherical zone with a
633 radius of r_ε , the deformation has a strain being equal to or exceeding a certain ε_s
634 which is smaller than the strain on the related fault. The r_ε is called the 'strain radius.'
635 They obtained $r_\varepsilon = 0.85(\varphi V \tau / \mu \varepsilon_s)^{1/3}$. This leads to
636

$$637 \quad \varepsilon_s = (0.85)^3 \varphi V \tau / \mu r_\varepsilon^3. \quad (22)$$

638

639 This reveals that the strain decreases when the radius or the distance from the
640 earthquake hypocenter increases. Based on Eq. (22), Rn concentration anomaly could
641 occur at a distance r_ε from the hypocenter when the strain at the observation site is
642 larger than ε_s . Hence, the pre-seismic strain in the related fault zone must be larger
643 than a particular value, ε_p ($> \varepsilon_s$), at time $t = t_p$. This makes the occurrence time of Rn
644 concentration anomaly be later than that of the pre-seismic strain because of $t_p > t_o$.
645 Thus, the precursor time of the former is shorter than that of the latter. Equation (5)
646 becomes

647

$$648 \quad \varepsilon(t) - \varepsilon_p = \{[a(\alpha-1)(t_f - t_p) + \varepsilon_{tf}^{1-\alpha}]^\eta - [a(\alpha-1)(t_f - t) + \varepsilon_{tf}^{1-\alpha}]^\eta\} / a(\alpha-2). \quad (23)$$

649

650 Define $T = t_f - t_p$ to be the precursor time of this precursor. Considering $\varepsilon_p = \gamma \varepsilon_{tf}$ and
651 $\varepsilon_{tf} \gg 1$, Eq. (23) hence becomes

652



653 $(1-\gamma)\varepsilon_f = \{[a(\alpha-1)T]^\eta/a(\alpha-2)\}. \quad (24)$

654

655 This yields

656

657 $T = [a(\alpha-2)(1-\gamma)\varepsilon_f]^{1/\eta}/a(\alpha-1). \quad (25)$

658

659 Taking the logarithm of the two sides of Eq. (25) leads to

660

661 $\log(T) = [a(\alpha-2)(1-\gamma)\varepsilon_f]^{1/\eta}/a(\alpha-1). \quad (26)$

662

663 This gives

664

665 $\log(T) = C' + AM_w \quad (27)$

666

667 where $C' = (1-\gamma)C < C$. This indicates that when the Rn concentration anomaly is taken
668 as a precursor, only the value of the constant is reduced from C to C' , while the
669 scaling exponent A does not change because of the same fault zone. This again to
670 confirm the importance of the $\log(T)-M$ relationship on the assessment of a
671 forthcoming earthquake. When two groups of earthquakes occur in two fault systems
672 whose rock materials have different values of a and α , their values of C and A could
673 be different, thus resulting in different $\log(T)-M$ relationships.

674 For Rn concentration anomalies before six earthquakes with $M=5.0-6.8$ and
675 $d=7.0-35.6$ km (M =the local magnitude; d =the focal depth, in km) in southeastern
676 Taiwan, Kuo et al. (2020) obtained $\log(T) = 1.456 + 0.053M$. For the Rn concentration
677 anomalies before 9 events in northern Taiwan, Wang (2023) obtained $\log(T) =$
678 $(-0.21 \pm 0.30) + (0.23 \pm 0.02)M$. For the Rn concentration anomalies before 111
679 earthquakes in Taiwan, Wang (2021b) obtained $\log(T) = (-2.05 \pm 0.40) + (0.58 \pm 0.01)M$
680 for the events with $d \leq 40$ km and $\Delta \leq 40$ km (Δ =the focal depth, in km); and $\log(T) =$
681 $(-0.40 \pm 0.42) + (0.26 \pm 0.01)M$ for those with $d > 40$ km or $\Delta > 40$ km. The $\log(T)-M$
682 relationship for northern Taiwan is different from that for southeastern Taiwan. This
683 indicates the difference on a of the fault-zone rocks between the two areas. The
684 $\log(T)-M$ relationship for northern Taiwan is different from those for Taiwan in two
685 different focal-depth ranges. This suggests that there is a difference on α of the



686 fault-zone rocks between northern Taiwan and the whole Taiwan region. That the
687 $\log(T)-M$ relationships for Taiwan in two different focal-depth ranges suggests that
688 the fault-zone rocks in the two different focal-depth ranges are different from each
689 other.

690 We assume that the theory proposed in this study can be applied to other kinds of
691 precursors, and thus the $\log(T)-M$ relationships exist for these precursors as
692 mentioned above. Based on the difference of the $\log(T)-M$ relationships between two
693 kinds of precursors, Wang (2023) suggested a method to predict the failure time and
694 magnitude of a forthcoming earthquake directly from observations. He explored in
695 details the conditions of the values of C' and A of Eq. (25) for two different
696 precursors that can be used for earthquake prediction. He also gave examples for
697 geochemical precursors to show how to predict the failure time and magnitude of a
698 forthcoming mainshock. The present theory provides the physical basis of his study.

699

700 **5. Conclusions**

701

702 From the subcritical crack growth model, we propose a theory of predicting a
703 forthcoming earthquake from pre-seismic strain signals. We consider three aspects:
704 prediction of failure time, prediction of earthquake magnitude, and prediction of
705 location. The pre-seismic strain is here considered as a fundamental and important
706 earthquake precursor. Based on the Voight's equation for failure of materials under
707 stresses, we theoretically investigate the physical basis on predicting the failure time
708 and magnitude of a forthcoming earthquake in terms of pre-seismic anomalous strain
709 signals which are generated on or near the fault where the event will happen.
710 Meanwhile, the present study demonstrates the physical basis of the $\log(T)-M$
711 relationships of precursors. Results exhibit that the failure time depends on the strain
712 rate and two parameters of the Voight's equation; while the magnitude are controlled
713 by the precursor time, two parameters of the Voight's equation, and the exponent of
714 the scaling law between the co-seismic strain and the fault length. The scaling
715 exponent, α , of the Voight's equation is an important factor on the $\log(T)-M$
716 relationship. Although the location of a forthcoming earthquake cannot be determined
717 from the present theory, it may still be qualitatively assessed from the observations.
718 The theory may be applied to the $\log(T)-M$ relationships of other kinds of precursors.



719 Based on the theoretical results made by Main (1998) and the observed values of A of
720 the relationships, the value of α must be in the range 1.0 to 1.8 for the generation of
721 earthquakes. The $\log(T)-M$ relationships of pre-seismic geoelectromagnetic and
722 geochemical signals are taken into account. Theoretical results reveal that the
723 precursor times of the pre-seismic geoelectromagnetic precursors and those of
724 geochemical precursors are, respectively, the same and shorter than that of the
725 pre-seismic strains.

726

727 *Data availability.* No

728

729 *Competing interests.* There are no known competing financial interests or personal
730 relationships that could have appeared to influence the work reported in this paper.

731

732 *Acknowledgments.* This study was supported by the Institute of Earth Sciences,
733 Academia Sinica, Taiwan, ROC.

734

735 **References**

736

737 Aki, K.: Ideal probabilistic earthquake prediction, *Tectonophys.*, 169, 197-198,
738 DOI:10.1016/0040-1951(89)90193-5, 1989.

739 Aki, K.: *Seismology of Earthquake and Volcano Prediction*. Science Press Beijing,
740 China, 331 pp (with Chinese translation), 2009.

741 Aki, K. and Richard, P.G.: *Quantitative Seismology*. H. Freeman and Co., San
742 Francisco, 932pp, 1980.

743 Atkinson, R.K.: Subcritical crack growth in geological materials, *J. Geophys. Res.*, 89,
744 4077-4114, 1984.

745 Atkinson, B.K.: Introduction to fracture mechanics and its geophysical applications,
746 In: Atkinson, B.K. (Ed.), *Fracture Mechanics of Rock*, 1-26, Academic Press,
747 London, 1987.

748 Atkinson, B.K. and Meredith, P.G.: Experimental fracture mechanics data for rocks
749 and minerals, In: Atkinson, B.K. (Ed.), *Fracture Mechanics of Rock*, Academic
750 Press. London, 477-525 1987.

751 Bak, P.: *How nature works: the science of self-organized criticality*. Springer



752 Science+Business Media, LLC, 212 pp, 1996.

753 Bernard, P.: Plausibility of long distance electrotelluric precursors of earthquakes, *J.*
754 *Geophys. Res.*, 97, 17531-17546, 1992.

755 Bishop, J.R.: Piezoelectric effects in quartz-rich rocks, *Tectonophys.*, 77, 297-321,
756 1981.

757 Bowman, D.D., Ouillon, G., Sammis, C.G., Sornette, A., and Sornette, D.: An
758 observational test of the critical earthquake concept, *J. Geophys. Res.*, 103,
759 24359- 24372, 1998.

760 Brace, W.F., Paulding, B.W. Jr., and Scholz, C.H.: Dilatancy in the fracture of
761 crystalline rocks, *J. Geophys. Res.*, 71, 3939-3953, doi:10.1029/J
762 Z071i016p03939, 1966.

763 Bufo, C.G. and Vanrnes, D.J.: Predicting modeling of the seismic cycle of the greater
764 San Francisco Bay region, *J. Geophys. Res.*, 98, 9871-9883, 1993.

765 Cornelius, R.R. and Voight, B.: Graphical and PC-software analysis of volcano
766 eruption precursors according to the Materials Failure Forecast Method (FFM), *J*
767 *Volcanol. Geotherm. Res.*, 64, 295-320, 1995.

768 Chen, K.C. and Wang, J.H.: On the studies of the May 10, 1983 Taipingshan, Taiwan
769 earthquake sequence, *Bull. Inst. Earth Sci., Acad. Sin., ROC*, 4, 1-27, 1984.

770 Chen, K.C., Wang, J.H., and Yeh, Y.L.: Premonitory phenomena of a moderate
771 Taiwan earthquake, *Terr. Atmos. Ocean. Sci.*, 1, 1-21, 1990.

772 Cianchini, G., De Santis, A., Di Giovambattista, R., Abbattista, C., Amoruso, L.,
773 Campuzano, S.A., Carbone, M., Cesaroni, C., De Santis, A., Marchetti, D.,
774 Perrone, L., Piscini, A., Santoro, F., and Spogli, L.: Revised accelerated moment
775 release under test: fourteen worldwide real case studies in 2014–2018 and
776 simulations, *Pure Appl. Geophys.*, 177, 4057- 4087, 2020.

777 Corson, D. and Lorrain, P.: *Introduction to Electromagnetic Field and Waves*,
778 Freeman, San Francisco, 552 pp, 1962.

779 Das, S. and Scholz, C.H.: Theory of time-dependent rupture in the earth, *J. Geophys.*
780 *Res.*, 86, 6039-6051, 1981.

781 De Santis, A., Cianchini, G., and Di Giovambattista, R.: Accelerating moment release
782 revisited: Examples of application to Italian seismic sequences, *Tectonophys.*,
783 639, 82-98, 2015.

784 De Santis, A., Marchetti, D., Spogli, L., Cianchini, G., Pavón-Carrasco, F.J.,
785 Franceschi, G.D., Di Giovambattista, R., Perrone, L., Qamili, E., Cesaroni, C.,



786 De Santis, A., Ippolito, A., Piscini, A., Campuzano, S.A., Sabbagh, D., Amoruso,
787 L., Carbone, M., Santoro, F., Abbattista, C., and Drimaco, D.: Magnetic field and
788 electron density data analysis from swarm satellites searching for ionospheric
789 effects by great earthquakes: 12 case studies from 2014 to 2016, *Atmosphere*,
790 10(7), 371, 2019.

791 Dieterich, J.H.: Preseismic fault slip and earthquake prediction, *J. Geophys. Res.*,
792 83(B8), 3940-3948, 1978.

793 Ding, G.y., Ma, T.c., and Ma, S.j.: Methods of earthquake prediction, In: *Earthquake*
794 *Prediction*, Evison, F.F. (Ed.), Terra Scientific Publishing Co., Tokyo, Unesco,
795 Paris, 453-465, 1985.

796 Dobrovolsky, I.P., Zubkov, S.I., and Miachkin, V.I.: Estimation of the size of
797 earthquake preparation zone, *Pure Appl. Geophys.*, 117, 1025-1044, 1979.

798 Enomoto, Y.: Coupled interaction of earthquake nucleation with deep Earth gases: a
799 possible mechanism for seismo-electromagnetic phenomena, *Geophys. J. Int.*,
800 191, 1210-1214, 2012.

801 Freund, F.: Charge generation and propagation in igneous rocks, *J. Geodyn.*, 33,
802 543-570. doi:10.1016/S0264-3707(02)00015-7, 2002.

803 Fu, C.C., and Lee, L.C.: Continuous monitoring of fluid and gas geochemistry for
804 seismic study in Taiwan, In: *Pre-Earthquake Processes: A Multidisciplinary*
805 *Approach to Earthquake Prediction Studies*, Ouzounov, D., Pulinets, S., Hattori,
806 K., and Taylor, P. (Eds.), *Geophysical Monograph Series*, 234, 199-218, 2018.

807 Fujinawa, Y., Noda, Y., Takahashi, K., Kobayashi, M., Takamatsu, K., and
808 Natsumeda, J.: Field detection of microcracks to define the nucleation stage of
809 earthquake occurrence, *Intern. J. Geophys.*, 2013, 1-18, Article ID
810 651823, <http://dx.doi.org/10.1155/2013/651823>, 2002.

811 Geller, R.J.: Earthquake prediction: a critical review, *Geophys. J. Int.*, 131, 425-450,
812 1997.

813 Geller, R.J., Jackson, D.D., Kagan, Y.Y., and Mulargia, F.: Earthquakes cannot be
814 predicted, *Science*, 275, 1616-1617, doi:10.1126/science.275.5306.1616, 1997.

815 Gutenberg B. and Richter, C.F.: Earthquake magnitude, intensity, energy and
816 acceleration, *Bull. Seism. Soc. Am.*, 32, 163-191, 1942.

817 Gutenberg, B. and Richter, C.F.: Frequency of earthquakes in California, *Bull. Seism.*
818 *Soc. Am.*, 34, 185-188, 1944.

819 Gulia, L. and Wiemer, S.: Real-time discrimination of earthquake foreshocks and



820 aftershocks, *Nature*, 574(7777), 193-199, 2019.

821 Gutenberg, B. and Richter, C.F.: Magnitude and energy of earthquake, *Annali de*
822 *Geofisica*, 9, 1-15, 1956.

823 Hayakawa, M. and Hobara, Y.: Current status of seismo-electromagnetic for
824 short-term earthquake prediction, *Geomatics Natural Hazards Risk*, 1(2),
825 115-155, 2010.

826 Hayakawa, M., Ohta, K., Maekawa, S., Yamauchi, T., Ida, Y., Gotoh, T., Yonaiguchi,
827 N., Sasaki, H., and Nakamura T.: Electromagnetic precursors to the 2004 Mid
828 Niigata Prefecture earthquake, *Phys. Chem. Earth*, 31, 356-364, 2006.

829 Kanamori, H.: Mode of strain release associated with major earthquake in Japan, *Ann.*
830 *Rev. Earth Planet. Sci.*, 1, 213-239, 1973.

831 Kanamori, H.: Initiation process of earthquakes and its implications for seismic
832 hazard reduction strategy, *Proc. Natl. Acad. Sci. USA*, 93, 3830-3837, 1996.

833 Kanamori, H. and Anderson, D.L.: Theoretical basis of some empirical relations in
834 seismology, *Bull. Seism. Soc. Am.*, 65, 1073-1095, 1975.

835 Kanamori, H. and Heaton, T.H.: Microscopic and macroscopic physics of earthquakes,
836 In: Rundle, J.B., Turcotte, D.L., and Klein, W. (Eds.), *Geocomplexity and*
837 *Physics of Earthquakes*, *Am. Geophys. Monog.*, 120, 147-163, 2000.

838 Kilburn, C.R. and Voight, B.: Slow rock fracture as eruption precursor at Soufriere
839 Hills volcano, *Montserrat*, *Geophys. Res. Letts.*, 29, 3665-3668, 1998.

840 Knopoff, L.: Energy release in earthquakes, *Geophys. J.*, 1, 44-52, 1958.

841 Knopoff, L.: Earthquake prediction: The scientific challenge, *Proc. Nat. Acad. Sci.*,
842 *USA*, 93, 3719-3720 (1996)

843 Kostrov, B.V., Das, S.: Idealized models of fault behavior prior to dynamic rupture.
844 *Bull. Seism. Soc. Am.*, 72, 679-703, 1982.

845 Kuhn, T.S.: *The Structure of Scientific Revolutions*. The University of Chicago Press,
846 *USA*, 210 pp, 1962.

847 Kuo, C.L., Lee, L.C., and Huba, J.D.: An improved coupling model for the
848 lithosphere-atmosphere-ionosphere system, *J. Geophys. Res.: Space Phys.*, 119,
849 3189-3205, doi:10.1002/2013JA019392, 2014.

850 Kuo, C.L., Huba, J.D., Joyce, G., and Lee, L.C.: Ionosphere plasma bubbles and
851 density variations induced by pre-earthquake rock currents and associated
852 surface charges, *J. Geophys. Res.*, 116, A10317, doi:10.1029/2011ja016628,
853 2011.



854 Kuo, T., Chen, W., Ho, C., and Kuo Chen, H., Chiang, C.: In-situ radon volatilization
855 in an undrained fractured aquifer, Proc., 44th Workshop Geothermal Reservoir
856 Engineer., 11-13, Stanford Univ., Stanford, Cal., USA, Feb., 2019.

857 Kuo, T., Lin, C., Chang, G., Fan, K., and Cheng, W., Lewis, C.: Estimation of
858 aseismic crustal strain using radon precursors of the 2003 M6.8, 2006 M6.1, and
859 2008 M5.0 earthquakes in eastern Taiwan, *Nat. Hazards*, 53, 219-228, 2010.

860 Kuo, T., Chen, W., Ho, C., Kuo Chen, H., and Chiang, C.: Precursory behavior of
861 groundwater radon in Southeastern Taiwan: Effect of tectonic setting in the
862 subduction zone, *Pure Appl. Geophys.*, 177, 2877-2887, <https://doi.org/10.1007/s00024-019-02389-9>, 2020.

864 Leonard, M.: Earthquake fault scaling: Self-consistent relating of rupture length,
865 width, average displacement, and moment release, *Bull. Seism. Soc. Am.*,
866 100(5A), 1971-1988, 2010.

867 Lomnitz, C. and Lomnitz-Adler, J.: A framework for earthquake prediction, In:
868 *Earthquake Prediction: An International Review*, 575-578, 1981.

869 Madden, T.R. and Mackie, R.L.: What electric measurements can say about changes
870 in fault systems, *Proc. Natl. Acad. Sci., USA*, 93, 3776-3780, 1996.

871 Main, I.G.: Prediction of failure times in the earth for a time-varying stress, *Geophys.*
872 *J.*, 92, 455-464, 1988.

873 Main, I.G.: Applicability of time-to-failure analysis to accelerated strain before
874 earthquakes and volcanic eruptions, *Geophys. J. Int.*, 139, F1-F6, 1999.

875 Main, I.G. and Meredith, P.G.: Classification of earthquake precursors from a fracture
876 mechanics model, *Tectonophys.*, 167, 273-283, 1989.

877 Martin, R.J.: Is piezomagnetism influenced by microcracks during cyclic loading?, *J.*
878 *Geomag. Geoelectr.*, 32, 741-756, 1980.

879 Meredith, P.G. and Atkinson, B.K.: Stress corrosion and acoustic emission during
880 tensile crack propagation in Whin Sill dolerite and other basic rocks, *Geophys.*
881 *J.R. Astron. Soc.*, 75, 1-21, 1983.

882 Milne, J.: Seismic science in Japan, *Trans. Seism. Soc. Jpn.*, 1, 3-33, 1880.

883 Mizutani, H., Ishida, T., Yokokura, T., and Ohnishi, S.: Electrokinetic phenomena
884 associated with earthquakes, *Geophys. Res. Lett.*, 3, 365-368, 1976.

885 Molchanov, O.A. and Hayakawa, M.: Generation of ULF electromagnetic emission
886 by microfracturing, *Geophys. Res. Letts.*, 22(22), 3091-3094, 1995.

887 Namgaladze, A.A., Zolotov, O.V., Karpov, M.I., and Romanovskaya, Y.V.:



888 Manifestations of the earthquake preparations in the ionosphere total electron
889 content variations, *Nat. Sci.*, 4(11), 848-855, doi:10.4236/ns.2012.411113, 2012.

890 Ogawa, T., Oike, K., and Miura, T.: Electromagnetic radiation from rocks, *J. Geophys.*
891 *Res.*, 90, 6245-6249, 1985.

892 Ohta, K., Watanabe, N., and Hayakawa, M.: The observation of ULF emissions at
893 Nakatsugawa in possible association with the 2004 Mid Niigata Prefecture
894 earthquake, *Earth Planets Space*, 57, 1003-1008, 2005.

895 Ouzounov, D., Pulinets, S., Hattori, K., and Taylor, P. (Eds.): *Pre-Earthquake*
896 *Processes: A Multidisciplinary Approach to Earthquake Prediction Studies*. AGU
897 publication, 384 pp, 2018.

898 Papazachos, C.B., Karakaisis, G.F., Savvaidis, A.S., and Papazachos, B.C.:
899 Accelerating seismic crustal deformation in the Southern Aegean area, *Bull.*
900 *Seism. Soc. Am.*, 92(2), 570-580, 2002.

901 Potirakis, S.M., Hayakawa, M., and Schekotov, A.: Fractal analysis of the
902 ground-recorded ULF magnetic fields prior to the 11 March 2011 Tohoku
903 earthquake (Mw=9): discriminating possible earthquake precursors from space-
904 sourced disturbances, *Nat. Hazards*, 85, 59-86, <https://doi.org/10.1007/s11069-016-2558-8>, 2017.

906 Pulinets, S. and Ouzounov, M.D.: Lithosphere–Atmosphere–Ionosphere Coupling
907 (LAIC) model – An unified concept for earthquake precursors validation, *J.*
908 *Asian Earth Sci.*, 41, 371-382, 2011.

909 Pulinets, S., Ouzounov, D., Karelina, A., and Davidenko, D.: Lithosphere–
910 Atmosphere–Ionosphere–Magnetosphere Coupling – A Concept for Pre-
911 earthquake Signals Generation, In: Ouzounov, D., Pulinets, S., Hattori, K., and
912 Taylor, P. (Eds.), *Pre-Earthquake Processes: A Multidisciplinary Approach to*
913 *Earthquake Prediction Studies*, *Geophy. Monog. Series*, 234, 79-98, 2018.

914 Reid, H.F.: The mechanics of the earthquake, *Rept. State Earthquake Inv. Comm.*, The
915 California Earthquake of April 18, 1906, Washington, D.C., Carnegie Inst., 1910.

916 Rikitake, T.: Dilatancy model and empirical formulas for an earthquake area, *Pure*
917 *Appl. Geophys.*, 113, 141-147, 1975a.

918 Rikitake, T.: Earthquake precursors, *Bull. Seism. Soc. Am.*, 65, 1133-1162, 1975b.

919 Rikitake, T.: Classification of earthquake precursors, *Tectonophys.*, 54, 293-308,
920 1979.

921 Rikitake, T.: Earthquake precursors, In: Evison, F.F. (Ed.), *Earthquake Prediction*,



922 Terra Scientific Publishing Co., Tokyo, Unesco, Paris, 3-21, 1984.

923 Rikitake, T. and Yamazaki, Y.: The nature of resistivity precursor, Earthquake Pred.
924 Res., 3, 559-570, 1985.

925 Rudnicki, J.W.: Physical models of earthquake instability and precursory processes,
926 Pure Appl. Geophys., 126(2-4), 531-554, 1988.

927 Rundle, J.B., Klein, W., Turcotte D.L., and Malamud, B.D.: Precursory seismic
928 activation and critical-point phenomena, Pure Appl. Geophys., 157, 2165-2182,
929 doi:10.1007/PL00001079, 2000.

930 Sarkar, I.: Possible precursory accelerated Benioff strain in the region of Sistan Suture
931 Zone of Eastern Iran, Acta Geophysica, 59(2), 239-261, 2011.

932 Sasai, Y.: The piezomagnetic field associated with the Mogi model, Bull. Earthq. Res.
933 Inst., Tokyo Univ., 54, 1-29, 1979.

934 Sasai, Y.: Application of the elasticity theory of dislocations to tectonomagnetic
935 modeling, Bull. Earthq. Res. Inst., Univ. Tokyo, 55, 387-447, (in Japanese with
936 English abstract), 1980.

937 Savage, B., Komatitsch, D., and Tromp J.: Effects of 3D attenuation on seismic wave
938 amplitude and phase measurements, Bull. Seism. Soc. Am., 100(3), 1241-1251,
939 doi:10.1785/0120090263, 2010.

940 Schirripa Spagnolo, G., Bernasconi, S.M., Aldega, L., Castorina,
941 F., Billi, A., Smeraglia, L., Agosta, F., Prosser, G., Tavani, S., and Carminati,
942 E.: Interplay and feedback between tectonic regime, faulting, sealing horizons,
943 and fluid flow in a hydrocarbon-hosting extensional basin: The Val d'Agri Basin
944 case, Southern Italy, Earth Planet. Sci. Letts., 646,
945 118982, <https://doi.org/10.1016/j.epsl.2024.118982>, 2024.

946 Scholz, C.H.: The Mechanics of Earthquakes and Faulting. Cambridge Univ. Press,
947 Cambridge, UK, 439 pp, 1990.

948 Scholz, C.H., Sykes, L.R., and Aggarwal, Y.P.: Earthquake prediction: A physical
949 basis. Science, 181, 803-810, doi:10.1126/science.181.4102.803, 1973.

950 Shaw, C.H.: Magnitude and slip scaling relations for fault-based seismic hazard. Bull.
951 Seism. Soc. Am., 113(3), 924-947, <https://doi.org/10.1785/0120220144>, 2023.

952 Sibson, R.H.: Fault rocks and fault mechanisms, J. Geol. Soc. Landon. 133, 191-213,
953 1977.

954 Slifkin, L.: Seismic electric signals from displacement of charged dislocations,
955 Tectonophys., 224, 149-152, 1993.



956 Smith, W.D.: The b-value as an earthquake precursor. *Nature*, 289, 136-139,
957 doi:10.1038/289136a0, 1981.

958 Smith, W.D.: Evidence for precursory changes in the frequency-magnitude b-value,
959 *Geophys. J. R. astro. Soc.*, 86, 815-838, 1986.

960 Sornette, D.: Mechanochemistry: An hypothesis for shallow earthquakes,
961 In: Teisseyre, R. and Majewski, E. (Eds.), *Earthquake Thermodynamics and*
962 *Phase Transformation in the Earth's Interior*, 1st Edition, Cambridge Univ. Press,
963 Cambridge, UK, 674 pp, 2001.

964 Stauffer, D. and Aharony, A.: *Introduction to Percolation Theory*. Taylor and Francis,
965 London, 1994.

966 Thingbaijam, K.K.S., Mai, P.M., and Goda, K.: New empirical earthquake
967 source-scaling laws, *Bull. Seism. Soc. Am.*, 107(5), 2225-2246, 2017.

968 Tsubokawa, I.: On relation between duration of crustal movement and magnitude of
969 earthquake expected, *J. Geod. Soc. Japan*, 15, 75-88, (in Japanese), 1969.

970 Tsubokawa, I.: On relation between duration of precursory phenomena and duration
971 of crustal movement and magnitude before earthquake, *J. Geod. Soc. Japan*, 19,
972 116-119, (in Japanese), 1973.

973 Tsubokawa, I., Ogawa, Y., and Hayashi, T.: Crustal movement before and after the
974 Niigata earthquake, *J. Geod. Soc. Japan*, 10, 165-171, 1964.

975 Turcotte, D.L. and Schubert, G.: *GEODYNAMICS – Applications of Continuum*
976 *Physics to Geological Problems*. Wiley, 450 pp, 1982.

977 Turcotte, D.L., Newman, W.L., and Shcherbakov, R.: Micro and macroscopic models
978 of rock fracture, *Geophys. J. Int.*, 152, 718-728, 2003

979 Tzanis, A. and Vallianatos, F.: A physical model of electrical earthquake precursors
980 due to crack propagation and the motion of charged edge dislocations, In:
981 *Seismo Electromagnetics (Lithosphere–Atmosphere–Ionosphere–Coupling)*,
982 TerraPub, 117-130, 2002.

983 Vallianatos, F. and Tzanis, A.: Electric current generation associated with the
984 deformation rate of a solid: Preseismic and coseismic signals, *Phys. Chem. Earth*,
985 23, 933-938, 1998.

986 van Deelen, G.: U.S. earthquake early warning system gets a major upgrade, *Eos*,
987 105, <https://doi.org/10.1029/2024EO240363>, 2024.

988 Varnes, D.J.: Predicting earthquake by analyzing accelerating precursory seismic
989 activity, *Pure Appl. Geophys.*, 130, 661-686, 1989.



990 Venegas-Aravena, P., Cordaro, E.G., and Laroze, D.: A review and upgrade of the
991 lithospheric dynamics in context of the seismo-electromagnetic theory, *Nat.*
992 *Hazards Earth Syst. Sci.*, 19,
993 1639-1651, <https://doi.org/10.5194/nhess-19-1639-2019>, 2019

994 Voight, B.: A method for prediction of volcanic eruptions, *Nature*, 332, 125-130,
995 1988.

996 Voight, B.: A relation to describe rate-dependent material failure, *Science*, 243, 200-
997 203, 1989.

998 Wang, J.H.: The seismic efficiency of the 1999 Chi-Chi, Taiwan, earthquake, *Geophys.*
999 *Res. Letts.*, 31, L10613, doi:10.1029/204GL019417, 2004,

1000 Wang, J.H.: Effect of thermal pressurization on the radiation efficiency, *Bull. Seism.*
1001 *Soc. Am.*, 99(4), 2293-2304, 2009.

1002 Wang, J.H.: A review on scaling of earthquake faults, *Terr. Atmos. Ocean. Sci.*, 29(6),
1003 589-610, 2018.

1004 Wang, J.H.: A review on precursors of the 1999 M_w 7.6 Chi-Chi, Taiwan, earthquake,
1005 *Terr. Atmos. Ocean. Sci.*, 32(3), 275-304, doi:10.3319/TAO.2021.03.24.01,
1006 2021a.

1007 Wang, J.H.: A compilation of precursor times of earthquakes in Taiwan, *Terr. Atmos.*
1008 *Ocean. Sci.*, 32(4), 411-441, doi:10.3319/TAO.2021.07.12.01, 2021b.

1009 Wang, J.H.: Piezoelectricity as a mechanism on generation of electromagnetic
1010 precursors before earthquakes, *Geophys. J. Int.*, 224, 682-700, 2021c.

1011 Wang, J.H.: A physical basis of predicting the magnitude and failure time of a
1012 forthcoming earthquake, *Ann. Geophys.*, 66, 6, doi:10.4401/ag-8914, 2023,

1013 Wang, J.H., Chen, K.C., Leu, P.L., and Chang, C.H.: Precursor times of abnormal
1014 b-values prior to earthquakes, *J. Seismol.*, 20(3), 905-919, DOI:10.1007/s10950-
1015 016-9567-7, 2016.

1016 Wang, K., Chen, Q.F., Sun, S., and Wang, A.: Predicting the 1975 Haicheng
1017 earthquake. *Bull. Seism. Soc. Am.*, 96, 757-795, doi:10.1785/0120050191, 2006.

1018 Wells, D.L. and Coppersmith, K.J.: New empirical relationships among magnitude,
1019 rupture length, rupture width, rupture area, and surface displacement, *Bull.*
1020 *Seism. Soc. Am.*, 84(4), 974-1002, 1994.

1021 Whitcomb, J.H., Garmany, J.D., and Anderson, D.L.: Earthquake prediction:
1022 Variation of seismic velocities before the San Fernando earthquake, *Science*, 180,
1023 632, 1973.



1024 Whitworth, R.W.: Charged dislocations in ionic crystals, *Adv. Phys.*, 24, 203-304,
1025 1975.

1026 Wu, Y.H., Chen, C.c., Rundle, J.B., and Wang, J.H.: Regional dependence of seismic
1027 migration pattern, *Terr. Atmos. Ocean. Sci.*, 23(2), 161-170, 2012.

1028 Wyss, M., Aceves, R.L., and Park S.K.: Cannot earthquakes be predicted?, *Science*,
1029 278, 487-490, 1997.

1030 Yu, S.B., Kuo, L.C., Hsu, Y.J., Su, H.H., Liu, C.C., Hou, C.S., Lee, J.F., Lai, T.C.,
1031 Liu, C.C., Liu, C.L., Tseng, T.F., Tsai, C.S., and Shin, T.C.. Preseismic
1032 deformation and coseismic displacements associated with the 1999 Chi-Chi,
1033 Taiwan, earthquake. *Bull. Seism. Soc. Am.*, 91, 995-1012, 2001.

1034 Zaccagnino, D. and Doglioni, C.: The impact of faulting complexity and type on
1035 earthquake rupture dynamics. *Communications Earth & Environment*, 3,
1036 358, <https://doi.org/10.1038/s43247-022-00593-5>, 2022

1037 Zaccagnino, D., Vallianatos, F., Michas, G., Telesca, L., and Doglioni, C.: Are
1038 foreshocks fore-shocks?, *J. Geophys. Res.: Solid Earth*, 129(2), e2023JB027337,
1039 2024.

1040 Zolotov, O.V., Prokhorov, B.E., Namgaladze, A.A., and Martynenko, G.V.:
1041 Variations in the total electron content of the ionosphere during preparation of
1042 earthquakes, *Russ. J. Phys. Chem. B*, 5(3), 435-438, doi:10.1134/
1043 s1990793111030146, 2011.

1044 Zolotov, O.V., Namgaladze, A.A., Zakharenkova, I.E., Martynenko, O.V., and
1045 Shagimuratov, I.I.: Physical interpretation and mathematical simulation of
1046 ionospheric precursors of earthquakes at midlatitudes, *Geomagn. Aeron.*, 52(3),
1047 390-397, doi:10.1134/S0016793212030152, 2012.

1048



1049

1050

1051

1052

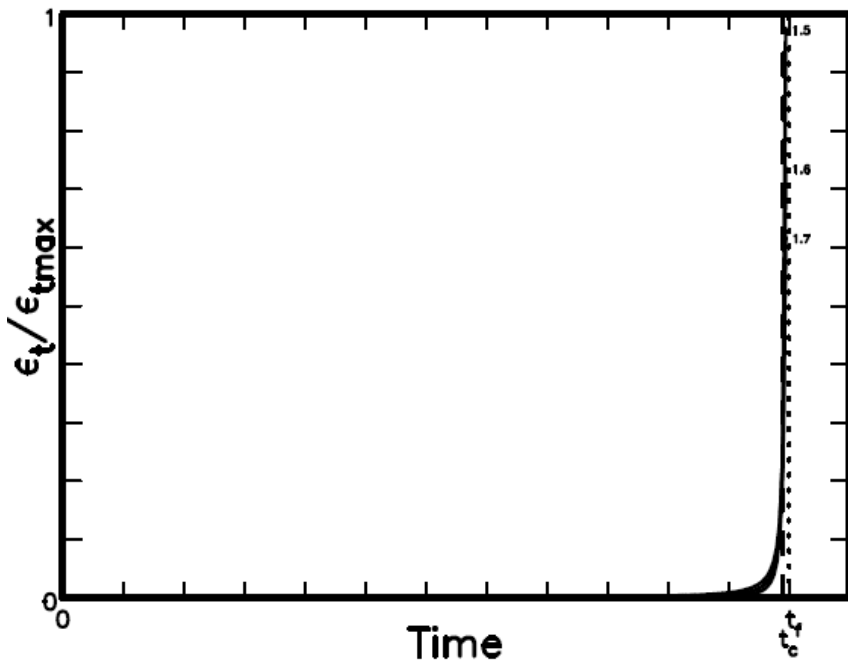
1053

1054

1055 Figure 1. The plot shows the time variations in strain rate, $\dot{\epsilon}_t(t)$, for $\alpha=1.5$, 1.6, and

1056 1.7 when $a=0.5$. The three curves intersect one another at the point with $t=t_c$.

1057





1058

1059

1060

1061

1062

1063

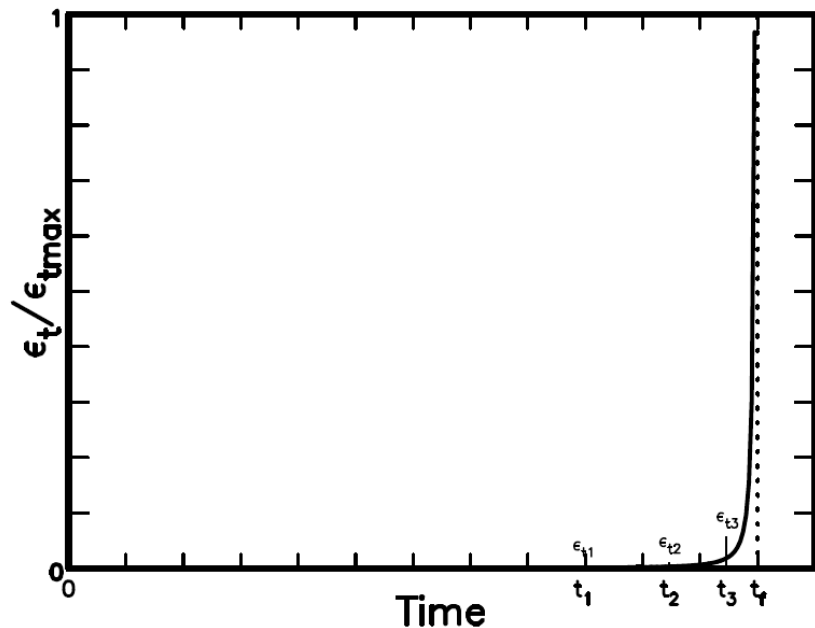
1064 Figure 2. The plot shows the time variation in strain rate, $\varepsilon_t(t)$, and three values of
1065 $\varepsilon_t(t)$, i.e., ε_{t1} , ε_{t2} , and ε_{t3} , at three time instants, t_1 , t_2 , and t_3 for $\alpha=1.6$ when
1066 $a=0.5$.

1067

1068

1069

1070





1071

1072

1073

1074

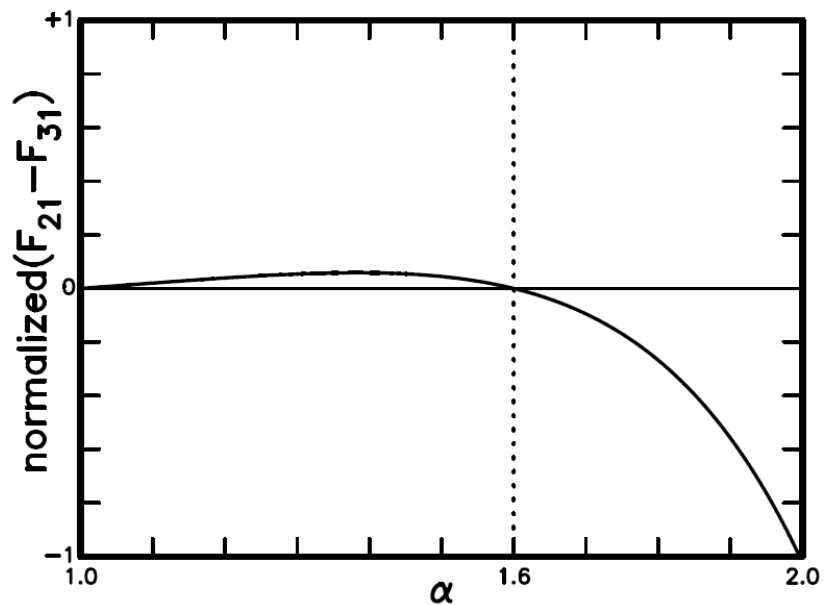
1075

1076

1077 Figure 3. The plot displays the curve for $F_{21}(\alpha) - F_{31}(\alpha)$. The intersection point of the
1078 curve and the line with $F_{21}(\alpha) - F_{31}(\alpha) = 0$ is at $\alpha = 1.6$.

1079

1080





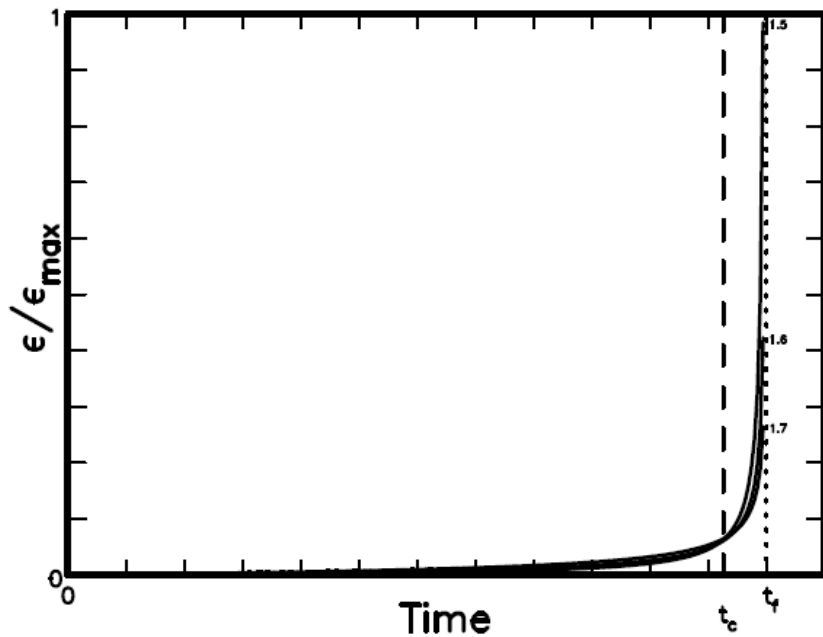
1081

1082

1083

1084

1085



1086

1087 Figure 4. The plot shows the time variations in strain, $\epsilon(t)$, for $\alpha=1.5$, 1.6, and 1.7
1088 when $a=0.5$. The three curves intersect one another at the point with $t=t_c$.